Understanding the Mechanism of Large-Scale Landslides

2

Runqiu Huang

We review recent work on large-scale landslide research that has been carrying out by the State Key Laboratory of Geohazard Prevention and Geoenvironment Protection, SKLGP. Based on intensive field investigations of large-scale landslides, several failure modes of gravitational and earthquake-induced landslides were proposed, which are widely applied in landslide hazard assessment and mitigation in China. For the gravitational landslides (including the rainfall-induced ones), a locking-section that resists landslide deformation has been commonly observed in many cases. The failure of the locking-section under the natural or human forces often causes the sudden failure of the whole slope, producing large-scale and high-speed landslides. Another failure mechanism "toppling" is not a new term, but the deep-seated large-scale toppling failures have been rarely studied. The slopes composed by anti-inclined lamellar weak strata or weak-hard rock intercalated strata are characterized by this type of failure. The toppling degree and stability are closed related to the strength and thickness of rock strata. The rock strata may experience large flexible bending deformations and failure only occurs when the deformation accumulates to a certain critical value. A deformation zone classification is proposed to assess the deformation stage and degree of toppling failure, which is also a key to evaluate the stability and mitigation of such type of landslides.

The research on landslides induced by the 2008 Wenchuan earthquake has also been reviewed. Based on the field investigation of more than 100 coseismic landslides, we found that these landslides had quite different characteristics from those produced under general gravity force. The head scarps of the coseismic landslides are serrated, rough, and steep due to the tensile stress, which are different from the smooth arc-shaped scarps of the gravitational landslide, caused by the shear stress. We found that tensile cracking, shattering and shearing are the basic failure components. The failure mechanism of most large-scale landslides can be explained by one mode or the combination of several modes. The aftershock monitoring and large-scale shaking table tests have been carried out to better understand the slope response to seismic wave. We found that factors contributing to susceptibility of a certain area to earthquake-induced landslides are distance from seismic fault, slope profile types, slope angle and elevation.

2.1 Introduction

China has vast territory (9.6 million km^2) with various topography types and geological structures. 67 % of the terrain is covered by mountains, plateaus, and hills, whereas basins and plains cover approximately 33 %. China is prone to different types of landslides due to anthropogenic activities and natural triggers. Some 400,000 landslides have been recorded in the last century, covering an area of 1.73 million km^2, accounting for 18 % of the total territory (Huang 2012). Since the 1980s landslide hazards have increased in China, probably due to the increase in construction activities and changes in climatic conditions (Huang and Chen 2004). The average rate of fatality caused by landslides is about 1,000 per year during the last 20 years (Li 1992; Schuster 1996; Wang 1999; Yin 2010). In addition to the loss of lives, they are also responsible for the loss of infrastructure, such as factories, mines, transportation routes, hydropower stations etc (Duan 2000; Jiang 2000; Yin 2001).

Liu et al (2013) created the temporal landslide inventory in the past 60 years, which shows that the hot spots of the high landslide potential areas, mostly concentrated in the southwest of China. As shown in Fig. 2.1, about 200 large-scale landslides are densely distributed around the Sichuan basin. This region is tectonically active because of its special location, the margin area of the Tibetan Plateau, where the intensive uplift of the Plateau since the Quarterly time resulted in a distinctive topographical contrast with the plateau and lower basins, high mountains and deeply incised

R. Huang (✉)
State Key Laboratory of Geohazard Prevention and Geoenvironment Protection, Chengdu University of Technology, Chengdu, China
e-mail: hrq@cdut.edu.cn

G. Lollino et al. (eds.), *Engineering Geology for Society and Territory – Volume 2*,
DOI: 10.1007/978-3-319-09057-3_2,

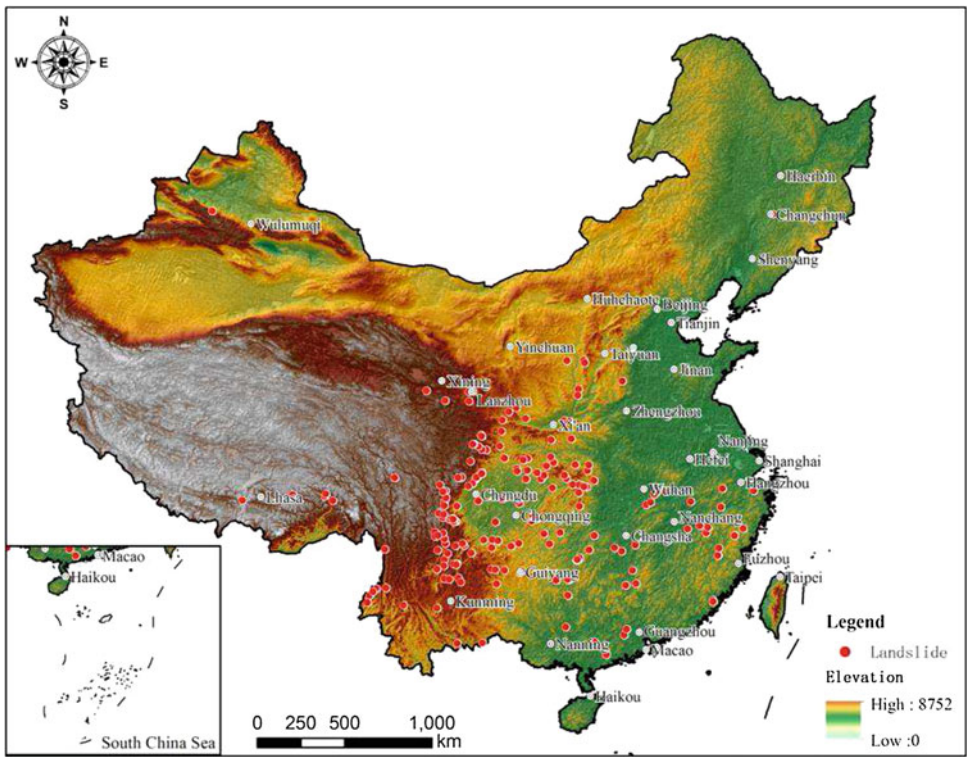

Fig. 2.1 Distribution of historical large-scale landslides in China (appendix A)

valleys. The collision between Indian and Europe–Asian plates also produced many active faults and high seismic activity. According to the latest report, there are 835 earthquakes with magnitude 4.7 or greater occurred in this region (Earthquake Disaster prevention department of China Earthquake Administration Bureau 1999). The recent notable examples are the 2008 Wenchuan earthquake and 2013 Lushan earthquake. The steep and rugged terrain, fragile geological environment and high seismic activity have caused a large number of landslides. The catastrophic landslides since the twentieth century in the southwest of China have been studied by Huang (2009). Chen et al. (2012) introduced several earthquake-trigger landslide events in this region and analyzed the relationship between the affected area of landslides and earthquake magnitude.

Landslide research in China mainly includes following directions:

- Fundamental research on landslide dynamics, mechanisms and processes using geotechnical, geophysical and numerical methods;
- Landslide mapping using various remotely sensed images and GIS techniques;
- Analysis of the spatial and temporal distribution of landslides based on multi-temporal landslide inventories;
- Landslide susceptibility, hazard and risk assessment and management;
- Landslide monitoring, early warning, forecast and mitigation;
- Landslide-induced secondary hazards, such as landslide dams (dam-break floods and debris flows), tsunamis and surges caused by submarine or reservoir landslides;
- Giant landslides triggered by large earthquakes or heavy rainfalls in different geological environments, such as rock avalanches, loess landslides, debris/mud flows etc.

It is not our intension to give a comprehensive review on above issues, as the number of literature is too many and is still growing. Rather we focus on the main findings of our group (the State Key Laboratory of Geohazard Prevention and Geoenvironment Protection, SKLGP) on the genetic and failure mechanism of gravitational and earthquake-induced landslides.

2.2 Gravitational Landslides

In southwestern China rapid uplifting of Qinghai-Tibet plateau during the Quaternary strengthens the downward incision of rivers, such as Lancang River, Nujiang River, Jinsha River, Yalong River and Dadu River, Minjiang River, forming a mountain and canyon landscape. The height of natural valley slopes normally reaches hundreds to thousands meters. Besides the high and steep topography, engineering geological conditions in this area are complex and typical of high geostress, high seismic intensity and strong weathering etc. Since 1970s, investigations into the deformation and failure of large-scale gravitational landslides

have been carrying out by senior generation of SKLGP (Zhang and Liu 1990). They found several mechanisms (i.e., creeping-tensile, sliding-bending, toppling, lateral spreading etc.), which can explain the deformation and failure of most of large-scale landslides. Based on these failure modes together with the investigation of landslides occurred in recent years, Huang (2012) proposed some new failure mechanisms: failure controlled by locking section and large-scale toppling. This section focuses on illustrating these two failure mechanisms and their role in slope stabilization and mitigation.

2.2.1 Deformation Mechanism with Locking Section Effect

It is important to define "locking section" at the first place. We consider any part of a slope resists to the slope failure as a locking section. Studies over the last 20 years indicate that the occurrence of large-scale rock landslides is normally closely related to sudden brittle failure of a locking section on the potential failure surface. It normally caused a sharp and rapid drop of the peak strength to residual strength of sliding surface, resulting in large-scale and high-speed landslides. The locking section is therefore extremely important to the deformation control and stability of a rock slope, which is the key to landslide hazard assessment and mitigation.

The failure mechanism controlled by locking section can be categorized into three modes, according to the location and effect of locking section in a slope (Table 2.1):

(1) Locking section formed during the deforming process of a slope

The locking section can be formed naturally with the deformation of a slope such as the sliding/tension-cracking-shearing failure mechanism in Table 2.1. It normally occurs in slopes that consist of (a) brittle rocks, or rock and soil, with near horizontal or gently inclined structural planes at the foot of slopes, and (b) hard rocks with thin interlayers of weaker material (i.e. the example shown in Table 2.1). The deformation process starts from the epigenetic deformation or creeping of a gentle dipping weak layer at the front of a slope, resulting in tension cracking at the rear part of the slope. The slope creeps continually under the long-term effect of gravity, causing the cracks in the upper part being further developed. There is a section in between of rear cracks and creeping weak layer, which has much less deformation or disturbance, and therefore hampering the slope failure. This section acts as a "locking section" in the slope. With the development of deformation in the rear and front of the slope, the stress at the locking section is gradually accumulated. Once the stress reaches to a certain value, it will cause the shearing failure of the locking section, finally leading to the brittle failure of slope, accompanied with considerable energy release. Landslides with this failure mechanism commonly produce "spoon" or "shovel"-shaped morphology.

The Zana and Longxi landslides which occurred near Longyangxia hydropower station on the Yellow River are typical examples with this failure mechanism (Zhang and Liu 1990). This mechanism was also found in the failures at the Laxiwa hydropower station on the Yellow River and the Yanchi phosphor mine in Hubei (Huang et al. 1993 and Huang 1996a, b). Based on a large number of case studies, Huang et al. (1993) found a statistical-empirical relation between the total slope height (H) and the critical depth of the crack in the rear of slope (H_{cr}): $H_{cr} = 0.5763H\text{-}27.0992$. It has been widely used to predict this type of slope failures.

(2) Locking section with high strength, acting like a "retaining wall" in the middle of a slope

As shown in Table 2.1, the basic characteristics of this kind of failure are: (1) the whole slope shows a relatively loose structure (strongly weathered zone), but there is a comparatively rigid geological body in the middle part of the slope, acting as a retaining wall; (2) the rigid part is normally pressurized by a strong force, caused by the deformation of the upper part. The function of the rigid part is the same as the "locking section", which plays a critical role in maintaining the stability of slopes (Huang et al. 1993; Huang et al. 2002a, b); (3) the front part is normally soft base consisting of mudstones or shales and therefore cannot provide much resistance; and (4) as the deformation develops abrupt brittle shear failure of the rigid part occurs, which leads to a high speed landslide.

This kind of landslide tends to occur in the following landforms: (1) the upper part of the slope is normally steep while the lower part is relatively flat, showing a concave profile; (2) the front part is composed of weak rock or soils; (3) the upper part usually develops structure planes nearly parallel to the slope surface; and (4) the middle part is comparatively hard but thin. A typical example is the Xikou landslide with a volume of 1.0 million m^3, occurred on July 10 of 1989 in Xikou of Sichuan Province. It was triggered by heavy rain, causing 221 deaths and 6 million Chinese Yuan economic losses. The upper part of the slope consisted of strongly weathered dolomite. The front part is Silurian mudstone. The central part is composed of high strength mudstone of Calcareous, which with high strength worked as a retaining wall withstanding the pressure from the upper part. The load transferred from the upper part to the lower part was restrained by the middle retaining wall. Thus the stress tended to be concentrated in this section. In time, the soft base below was compressed, and slowly crept towards the free face. Once the concentrated stress became greater

Table 2.1 Summary of landslide in locking section mode

Mode	Topography and geological features	Failure mechanism	Typical structure of the slope
Sliding-tension cracking-shearing	Slope consists of gently inclined layered rocks (dip angle <10°); There is a layer of soft rock at the toe; and The slope angle is greater than 35°	(1) Tension cracking occurs at the crest; and (2) creep deformation happens along at the toe of the slope; (3) shearing occurs at the middle part of the slope by shear	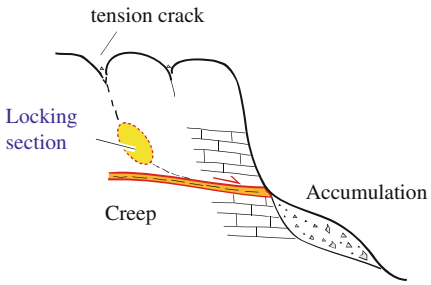
Retaining wall failure	The upper part is normally composed of weathered rocks. The front part is of soft rock. In the middle a comparably rigid block exists. The upper slope is steep, while the front part is relatively flat, forming a concave landform	(1) The upper slope creeps along the potential sliding surface. Its deformation is restrained by the rigid section in the middle; (2) the soft base in the front part gradually deforms due to gravity; and (3) accumulation of stress on the rigid section causes brittle failure of this part and subsequently the overall failure of the slope	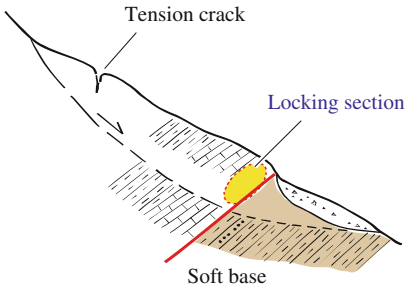
Key block failure	Rock layers incline inwards at a dip angle of about 15–30°; Slope usually contains a certain thickness of weak rock layer, whose friction angle lie between 15 and 25°	(1) The upper layer creeps and leads to tension cracks at the trailing part; (2) the key block is gradually lose strength by external actions, like engineering excavation and/or karst erosion; and (3) break up of the key block results in overall failure	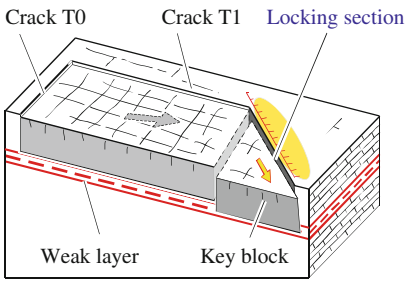

than the strength of the retaining wall section, an abrupt brittle failure occurred.

A visco-elastic–plastic non-linear finite element method was used to simulate and validate the above mechanism. Figure 2.2a shows that the surface displacement in the middle of the slope is less than that in the upper and lower parts of the slope. The deformation in the upper part of the slope can reach several tens of centimeters, while the deformation in the locking section is usually smaller. Consequently, the deformation of the upper part will be restricted by the locking section, while the stresses and strains caused by the sliding force of the upper part will accumulate in the locking section. Correspondingly, accumulation and transmission of the maximum principal stresses of different parts of the slope vary with time (Fig. 2.2b); the stresses in the locking section increase with time while those in the lower part (the soft base) do not change initially but decrease after a certain period of time, thus imposing higher stresses in the locking section.

(3) Locking section in the front of slope as a key block controlling the slope deformation

This type of failure is similar to the "retaining-wall" mechanism. The difference is that it usually occurs in gently inclined bedrock slopes with the locking section in the front of slope and acting as a "key block". The slope may be composed of intercalated weak and strong rocks. The upper part gradually creeps along a weak layer, while the creep is restrained by the key block (Table 2.1). Failure of the key block due to human engineering activities and natural deformation processes will cause the overall failure of slope.

A representative example is the Jiweishan landslide occurred on June 5, 2009 in Wulong, Chongqing, causing 74 fatalities (Yin 2010). The upper layer of the rock mass is

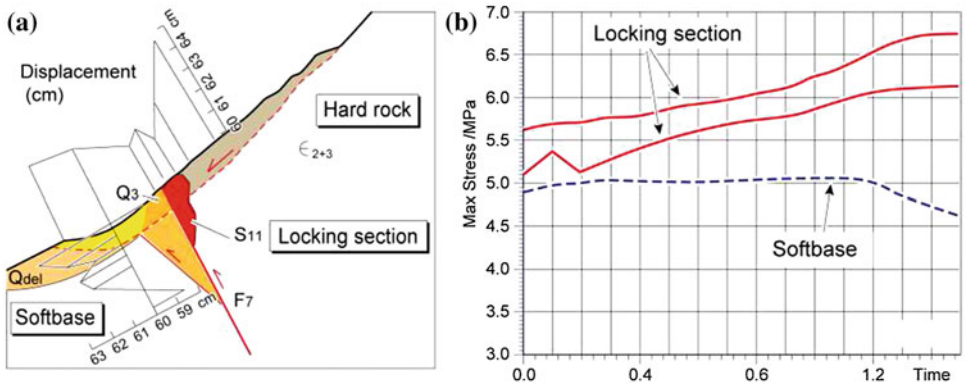

Fig. 2.2 The deformation and stress variation in the locking section

limestone, below which is bituminous limestone underlain by hydromica clay rocks. The trailing crack T0 is 152 m long, 60–70 m deep, and the lateral crack T1 is 530 m long (in Table 2.1). The thickness of displaced rock mass is about 60 m. The limestone layer creeps along the underlying weak bituminous shale towards the key block, forming a huge driving force. The triangle-shaped block in the front was suffered from karst dissolution. With the increase of driving force and the decrease of the resistance by the key block, sudden brittle failure happened.

2.2.2 Toppling Deformation and Failure

Toppling failure is not new, which has been commonly found in shallow rock falls. However, little is known about the deformation and failure mechanism of deep-seated large-scale topping landslides. Few people believe that large-scale landslides can occur in slopes with counter-inclined rock strata. The common thinking is that the toppling deformation can only occur from the surface to several tens of meters depth in anti-inclined strata (Zhang and Liu 1990; Wang 1992). In the last 20 years, however, 200–300 m deep bending and toppling deformations have been recorded in southwest China (Fig. 2.3), resulting in large-scale and deep landslides. According to an incomplete statistics, landslides occurred in anti-inclined strata account for 33 % of total landslides happened in recent years in China.

2.2.2.1 Types of Deep-Seated Toppling

The deep-seated toppling failure can be classified into three types as listed in Table 2.2, where the geological conditions, failure processes and typical structures for each mode are provided.

(1) Toppling in interlayered rock slopes

This type of failures commonly occurs in slopes composed of layered metamorphic sandstone, slate and carbonaceous slate, phyllite with silk mica schist, especially in Songpan-Ganzi geosyncline area, Qinling metamorphic rock series,

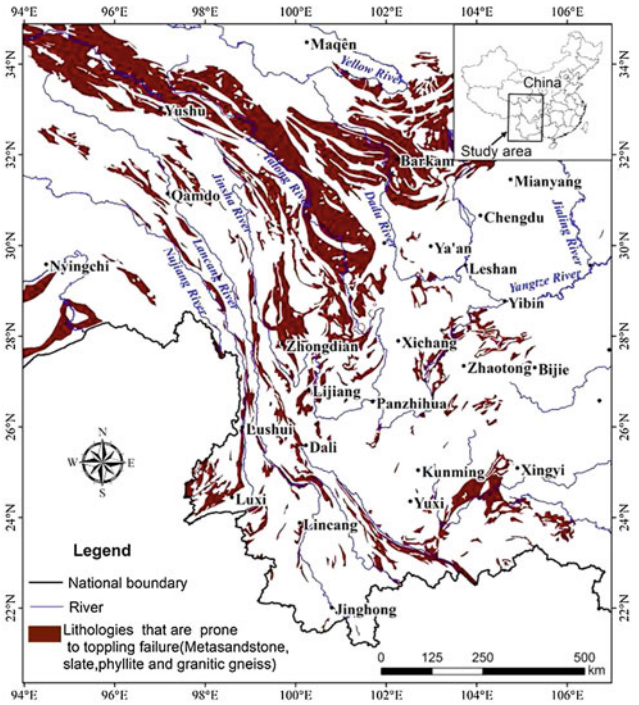

Fig. 2.3 Strata susceptible to toppling in southwest China

etc. (Fig. 2.3). For example, large-scale toppling deformation occurred in a 10 km wide zone of Triassic metamorphic sandstone and slate slopes along the Yalong River. The deformation area, with a horizontal depth of almost 300 m (Fig. 2.4), is located on the left bank of the first stage of the Jinping Hydropower Station, although the rock slopes on both banks of the river toppled toward the river some 10 km upstream of the station. This toppling deformation caused two large landslides: the Shuiwen station landslide and the Jiaba landslide.

In this area the slopes are almost vertical and the strata dip 85°–87° towards the N10°–30° E (Fig. 2.4). The bottom of the strata is mainly composed of dark grey, thinly layered sandy slate of Triassic age. The middle and top parts of the strata are mainly thin layers of greyish-green schist, marble and some sandstone. According to the data from the

Table 2.2 Summary of landslides in toppling deformation mode

Mode	Topography and geological features	Failure mechanism	Typical features of the slope
Toppling in interlayered rock slopes	Rock mass is composed of soft and hard rock layers; The strata dip inwards the slope at the angle of 40–60°. The slope is steep (normally 25–40°)	(1) Vertical or sub-vertical rock layers bend due to gravity; (2) The bending can extend to a great depth due to the flexibility of the strata; and (3) Shear plane would be developed in some depth to form a landslide	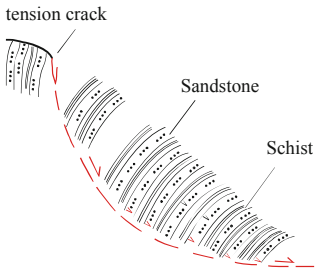
Toppling due to weak base	Slope usually consists of two sections: the upper section is composed of hard rock, while the lower part is relatively soft rock working as a soft base; The dip angle of the strata is between 35 and 50°. The slope normally shows a concave pattern with a steep upper part and a gentle lower part	(1) The upper part suffers toppling; (2) The lower part creeps under compression by the upper part, leading further toppling of the upper; and (3) The upper part is eventually failed through the potential sliding surface, and then cuts through the lower weak formation base	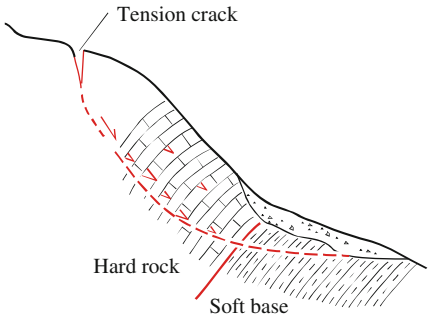
Toppling and sliding	The upper part of the slope usually consists of hard rock, while the lower part soft rock. A set of joints in the upper part dips outwards the slope	(1) The lower soft base would deform due to the gravity of overlying rock mass; (2) This deformation introduces the upper part to be dislocated along the joints; and (3) Once the dislocation develops to a great extent, landslide happens	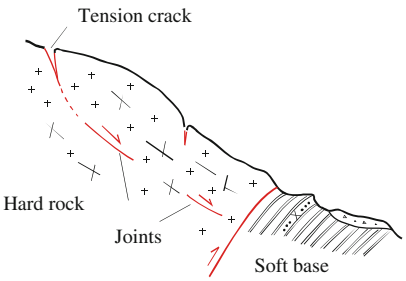

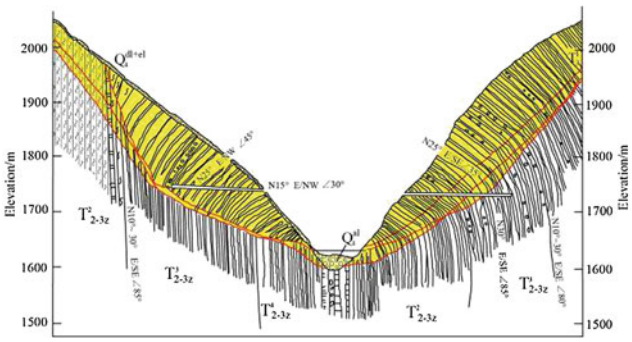

Fig. 2.4 Engineering geological profile of Shuiwen station site in Yalong river (unit: m) (Wang et al. 1995)

horizontal tunnel (ZD1), the toppling deformation of the strata was very severe.

The failure mechanism is ready to understand, as weak perpendicular planes are flexible to bend towards free surface. Investigations indicate that toppling deformation occurred in all steep slate and schist strata, although the toppling degree and scale varied from one slope to another.

(2) Toppling due to weak base

In the case where a soft base lies at the toe of the slope, long-term compression produces non-uniform downwards deformation, causing the slope to suffer from the overturning moment and leading to outward toppling (Table 2.2). Tension cracks may develop to some depth at the trailing edge of the slop body. Water filling in these cracks may further favor the overturning moment to exaggerate the toppling.

The vertical cliff in Fig. 2.5 is about 170 m high, consisted of thickly bedded limestone, underlain by mudstone (the weak base), which is covered by colluvium deposits. Large-scale cracks were found at the top within a distance of about 40 m from the slope crest. These cracks are parallel to the slope surface. Cracks L1, L2, L7 have an average width (aperture) of 0.5–1.5 m, locally 2.0–3.0 m, filled with soil

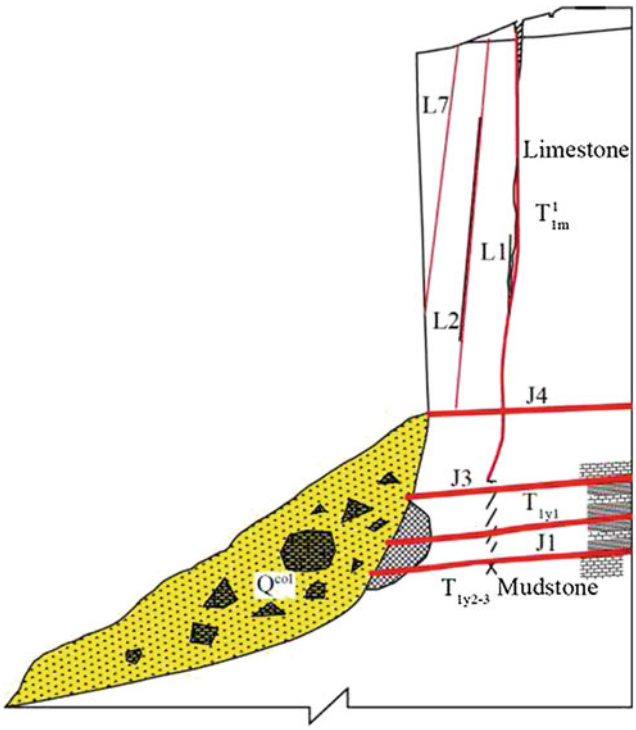

Fig. 2.5 Toppling of limestone due to the soft base of mudstone

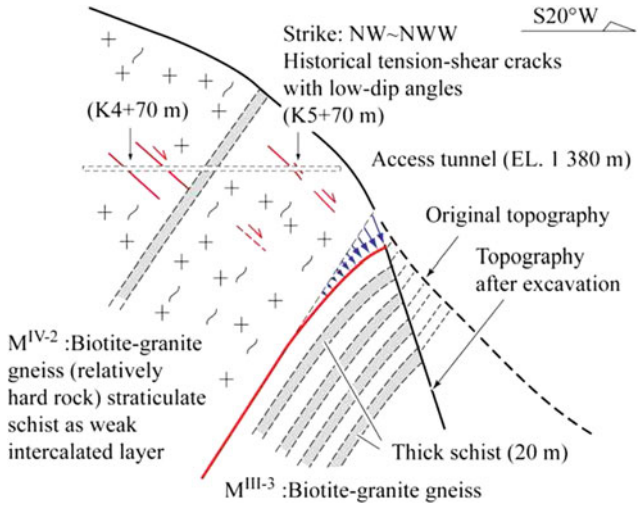

Fig. 2.6 High slope of Xiaowan hydropower station

and rock fragments. Compression-induced extrusion of mudstone at the toe can be found. These facts indicate an outwards deformation has been developed due to contraction of mudstone pressurized by gravity of rock mass on top of it. This finally results in the upper rocks to topple.

According to case study investigation, the following geological and topographic marks can be used to identify toppling deformation due to soft base: (a) the upper part of the slope usually consists of hard rocks; (b) at the slope toe a soft base exists and mostly consists of mudstone, carbonaceous slate, schist etc.; (c) the upper part of the slope is almost vertical; and (d) large tension cracks can be found in the trailing edge of the slope body.

(3) Toppling and sliding

In the case where slopes with a set of joints parallel to the slope surface, both toppling and sliding would happen (Table 2.2). The rock layers tend to topple under gravity and slipping along the joints. As the length of joints is normally limited or restrained by rock layers, an obvious tension-induced crack structure is rarely to be found at the rear part of the slope. Instead, they look more like unloading cracks. Generally, engineering excavation would introduce deformation of this kind, especially deformation along the pre-existing unloading-induced cracks. Figure 2.6 shows a high rock slope in the dam site of Xiaowan hydropower station. The height of the slope is about 180 m. The upper part is composed of biotite-granite gneiss with schist, while the lower part is schist of 20 m thick, which acts as a weak base of the slope. The rock layers dip inwards the slope with a set of structural plane dipping at the same direction of the slope surface (40°–50°). Under engineering excavation, deformation was developed in the soft base due to compression by the gravity of the upper part. Consequently, the upper rock mass dislocate itself along the joints. The deformation ceased once the excavation stopped.

Note that different from cataclinal rock slopes that normally slide along an existing potential failure plane (i.e. a weak layer, structural plans etc.), the sliding plane of toppling slopes is formed during the slope deformation process. Therefore, the failure may take a long incubation period, especially for flexible rock mass. The rock strata may experience large flexible bending deformations and failure only occurs when the deformation accumulates to a certain critical value.

2.2.2.2 Classification of Deformation Zones in Deep-Seated Toppling Slopes

According to the extent toppling deformation develops, the rock mass within a slope can be divided into four zones (a, b, c and d) from the outer to the inner part of the slope (Fig. 2.7).

A lot of facts indicates that the dip angle of the bed rock (Zone E) determines the depth of toppling. As shown in Fig. 2.8, the geo-mechanics modelling tests reveal strata with dip angle of between 60°–70° are the most susceptible to toppling. According to field survey, it is indicated that the toppling grade can be divided into 4 classes, as shown in Table 2.3. Table 2.4 lists the main features and quantitative parameters of layered rocks for different toppling grades. It is found that the tension scale in mm and unit tension are all increased with degree of toppling.

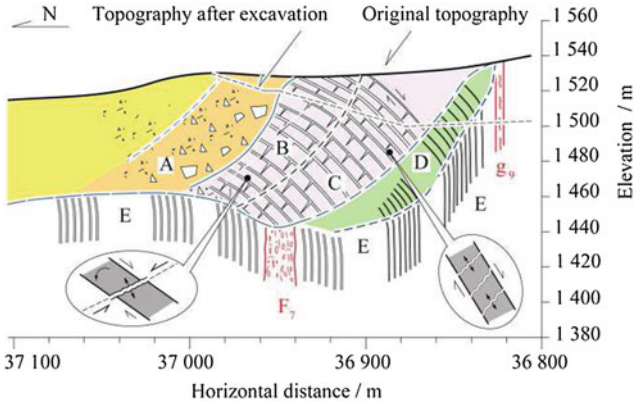

Fig. 2.7 Toppling deformation structure at Xiaowan hydropower station on Lancang River: **a**. Falling and decompostion; **b**. Stronly toppling; **c**. Moderately toppling; **d**. Slightly toppling; E. Bed rocks

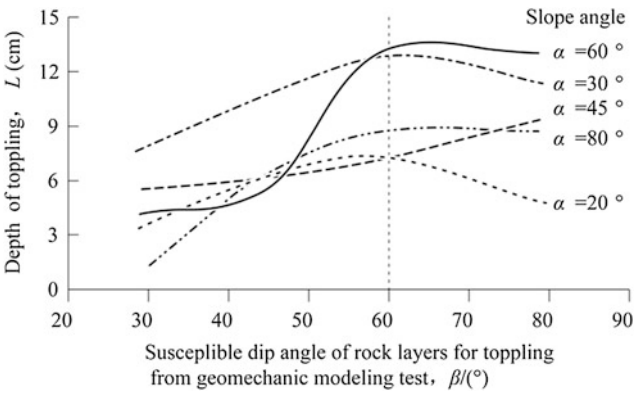

Fig. 2.8 Dip angle influences the depth of toppling deformation

The toppling deformation is closely related to the strength and thickness of rock strata. For the toppling occurs in hard lamellar rock mass, the deformation depth is normally between 30 and 40 m. Unlike the deformation of soft strata, in hard lamellar rock the deformation involves bending of the joints and cracks. In soft rock mass, there is a long deformation time from the beginning to the slope failure, and the degree of toppling can be very large. During the deformation process, the slope stability is not particularly low. In contrast, the hard rock strata fail very shortly after the slope begins to deform.

As aforementioned, the toppling failure does not occur along an existing sliding plane like that in cataclinal slopes. Therefore, the limit equilibrium method commonly used to estimate slope stability is not suitable to slopes with deep-seated toppling failure mechanism. The classification of deformation zones of toppling failure helps to assess the deformation stage and stability of slopes, which has been used in dam construction in China. It is also significantly important for determining the control measures of topping failures. For example, if anchors are used to stabilize a slope, the anchoring section should be placed in the Zone C or D.

2.3 Earthquake-Triggered Landslides

Strong earthquakes are among the prime triggering factors of landslides (Keefer 1984). The 2008 Wenchuan earthquake (Mw 7.9, China) highlighted the importance of assessing and mitigating the coseismic landslides and the consequent secondary hazards. The earthquake was the largest seismic event in China in more than 50 years, causing 69,227 fatalities and 374,643 injured (Yin et al. 2009). Apart from the direct damages, the earthquake triggered around 60,000 landslides (Dai et al. 2011; Gorum et al. 2011), among which more than 800 blocked rivers, forming landslide dams (Fan et al. 2012a). It occurred on the NE-trending Longmen Shan thrust fault zone at a focal depth of 14–19 km, which separates the Sichuan basin from the steep and heavily dissected eastern margin of the Tibetan Plateau in China. This fault zone consists of three major sub-parallel faults: the Wenchuan-Maowen, Yingxiu-Beichuan and Pengguan faults. The coseismic rupture initiated near Yingxiu town (31.061°N, 103.333°E) and propagated unilaterally towards the northeast, generating a 240-km long surface rupture along the Yingxiu Beichuan fault, and a 72-km long rupture along the Pengguan fault (Xu et al. 2009a, b, c, d; Lin et al. 2009; Shen et al. 2009).

In this section, we briefly review the research that SKLGP has done on the geohazards associated with the Wenchuan earthquake, with focus on the failure mechanism and controlling factors of the coseismic landslide occurrence.

2.3.1 An Overview of Our Research in the Past Five Years

The State Key Laboratory of Geohazard Prevention (SKLGP), with which the authors are working, has continued investigating the landslides and post-earthquake debris flows towards a better seismic hazard assessment and management. Shortly after the earthquake, our lab made the preliminary coseismic landslide mapping of 11,308 landslides by visual interpretation of RS images and field investigation in the accessible regions. Based on this inventory, Huang and Li (2009a) analyzed the general distribution pattern and controlling factors of coseismic landslides, revealing that the distance to fault surface rupture and hanging-wall effect are the most significant factors; while the further study (Huang and Li 2009b) found that local geomorphology and topography also play a crucial role in determining the occurrence of earthquake-induced landslide, as slope crests, the transition section of slope gradients and

Table 2.3 The classification of toppling

Description	Falling and deposition, Zone A	Strongly toppling, Zone B	Moderately toppling, Zone C	Slightly toppling, Zone D	Mother rock, Zone E
Decomposed	Highly decomposed	Strongly decomposed, tension cracks and shearing developed within layer	Bending with shearing along layers	Slightly bending	Null
Weathering degree	Completely weathered	Highly weathered	Moderately weathered	Slightly weathered or fresh	Fresh rock

Table 2.4 The physical parameters of rocks with different toppling grades

Grade of toppling	Features	Change of dip angle of rock strata	Width of Tension scale (mm)	Unit tension mm/m
Zone A	Rock fall	>40º–60º	50.0–100.0	30.0–50.0
Zone B	Tension crack and Shearing along the tension cracks, shearing between rock layers	20º–40º	20.0–50.0	15.0–30.0
Zone C	Tension cracks, shear of rock layers	10º–20º	5.0–20.0	5.0–15.0
Zone D	Little shear deformation along bedding planes. No obvious tension crack	05º–10º	0 < 5.0	<5.0

thin mountain ridges were observed to be generally susceptible to such landslides. Gorum et al. (2011) created one of the most complete inventories, including 60,000 coseismic landslides. Tang et al. (2011) carried out landslide hazard assessment in Beichuan, using an index-based approach. Xu et al. (2009a) studied the characteristics of some large-scale landslides triggered by the Wenchuan earthquake. Huang et al. (2012) depicted the geological and geomorphological features of the largest coseismic landslide, the Daguangbao landslide, and also estimated its failure mechanism. Shaking table tests were carried out in order to analyze slope behavior under seismic loading. Xu et al. (2009b) revealed that the typical deformation and failure mode of the slope rock mass under strong shock are mainly of the tensile failure. Huang et al. (2013) compared the response of anti-dip hard rock slopes and soft rock slopes by large scale shaking table tests. The results indicated that deformation mainly developed at a shallow depth in the upper part of the hard rock slope and in the upper (near the crest) and lower (near the toe) parts of the soft rock slope.

The cascading effect of landslides such as river damming and subsequent floods has also been our research focus. Xu et al. (2009c) qualified the hazard of these 32 dams by considering dam height, dam composition materials and maximum capacity of the landslide-dammed lakes. Fan et al. (2012a) created an almost complete landslide dam inventory that consists of more than 500 landslide dams. Among them, the most dangerous one is the Tangjiashan landslide dam that impounded a lake with an estimated volume of 3×10^7 m^3. Before being breached, it posed a serious threat to 2.5 million people downstream, especially in the city of Mianyang, located 85 km downstream. Fan et al. (2012b) simulated dam-breach flood scenarios of the Tangjiashan landslide dam using an integrated approach that combines the physically-based BREACH model and the 1D-2D SOBEK hydrodynamic model. The decay of landslide dams and barrier lakes was quantified by Fan et al. (2012c), indicating that about one-quarter of the dams induced by the Wenchuan earthquake failed within one week and 60 % within 1 month after the earthquake. The reader is referred to Fan (2013) for an overview of the landslide dam research.

A large amount of loose sediment from coseismic landslides has promoted post-earthquake debris flow occurrence, which has become a significant concern. Tang et al. (2011) investigated the landslides and debris flows induced by the first heavy rainfall four months in Sep, 2008 after the earthquake in the Beichuan region. Xu et al. (2012) studied the debris flows triggered by another heavy rainstorm that occurred during 12–14 August 2010, including the Wenjia gully and Zoumaling gully debris flows in the Qingping catchment, the Hongchun gully debris flow near the town of Yingxiu and the Longchi debris flow near Dujiangyan city. The most catastrophic Wenjia debris flow delivered 450×106 m^3 sediment into the Mianyuan river, causing the river blockage and flooding of the Qingping town (Tang et al. 2012). Zhou et al. (2014) found that the rainfall threshold for triggering debris flows increase each year based on the rainfall data of 14 debris flow events after the earthquake.

To summarize, Huang (2011) concluded the geo-engineering lessons that we have learned from the Wenchuan earthquake, giving recommendations for coping with large-scale geohazards and reconstruction site selection. Another overview has been made by Huang and Fan (2013), who

pointed out that focused research efforts must be invested into quantifying the impact cascade following a large earthquake, especially the long-term effect.

2.3.2 Failure Mechanism and Modes of Earthquake-Triggered Landslides

Based on the field investigation of more than 100 large-scale landslides triggered by the Wenchuan earthquake, we found that these landslides had quite different characteristics from those produced under general gravity force. The head scarps of the coseismic landslides are serrated, rough, and steep due to the tensile stress, which are different from the smooth arc-shaped scarps of the gravitational landslide, caused by the shear stress. This might be because:

(1) *Under normal gravity conditions*

The stress state in the superficial part can be described as followed: the maximum principal stress is parallel to the slope surface; the minimum principal stress is vertical to the slope surface; the intermediate principal stress is parallel to the strike direction of slope. Therefore, the shear stress concentration occurred at weak surface and slope toe part, which resulted in shear deformation and failure following Morh-Coulomb criterion along the weak plane, i.e. weak structural plane or the ancient sliding surface. With shear deformation developed, an apparent tensile stress concentrated at the trailing edge of the slope, and resulted in many tensile cracks (Fig. 2.9a).

(2) *Under the seismic loading conditions*

During the earthquake, the minimum principal stress of the slopes is performed as a repeated pull-compressive stress state on the influence of seismic waves. Due to the elevation amplification effect, the horizontal acceleration in the upper part of the slopes is always larger than 1 g. Thus, the seismic horizontal inertia force is far more than the tensile strength of rock mass itself. Griffith proposed a criterion of crack propagation, i.e., $\sigma_s > \sigma_\tau$, which illustrated that the rock mass of slope are prone to generate the crack surface parallel to the free surface under seismic conditions. Sustained shaking will contribute to widen and deepen the crack surface during the earthquake, resulting in the formation of a deep tension crack parallel to the strike direction at the top of the slope. Subsequently, crack-shear slip surface will develop at the bottom of the slope and landslide happened eventually (Fig. 2.9b).

Fundamentally, earthquakes affect the stability of slopes in two ways. First, the ground shaking may reduce the frictional strength of the substrate by shattering of rock mass or liquefaction. Second, the seismic acceleration may result in short-lived and episodic changes of the normal (tensile) and shear stresses in the hillslopes during earthquakes. We found that the strong shaking (the seismic acceleration) plays a significantly important role in the early stage of landslide failure, since it generated the tensile stress, causing the tensile cracking in the rear of the slope. The ground shaking can also cause the shattering of rock mass, reducing the frictional strength of the substrate in this way.

Due to the high magnitude, long duration, strong ground shaking and fragile geo-environment in the mountainous region, the coseismic landslides show some special initiation and runout phenomena, which are difficult for people to describe using the existing landslide terms. Therefore, based on a large amount of on-site investigations, several new terms had to be defined, such as tensile-cracking, shattering-sliding, shattering-falling, and ejection, in order to vividly describe the basic dynamic deformation process and characteristics of the coseismic landslides (Huang 2011 and Xu et al. 2013). We present a brief explanation of following basic failure modes. The failure mechanism of most large-scale landslides can be explained by one mode or the combination of several modes.

(1) *Tensile cracking*

This failure mode assumes that when the seismic wave propagates to discontinuities in rock slopes, it may cause the tension stress at interfaces and form the tension fractures, because the horizontal seismic force may enormously exceed the tension strength of the rock mass. This assumption explains the appearance of precipitous or erect back scarps in most of large-scale coseismic rockslides, such as the head scarp and vertical cracks in the Daguangbao landslide (Fig. 2.10).

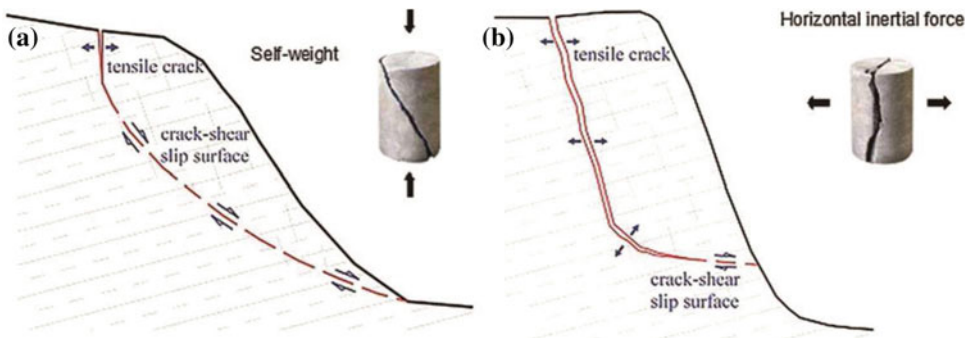

Fig. 2.9 Typical deformation and failure mode of rock slope under normal gravity conditions (**a**) and under seismic loading (**b**)

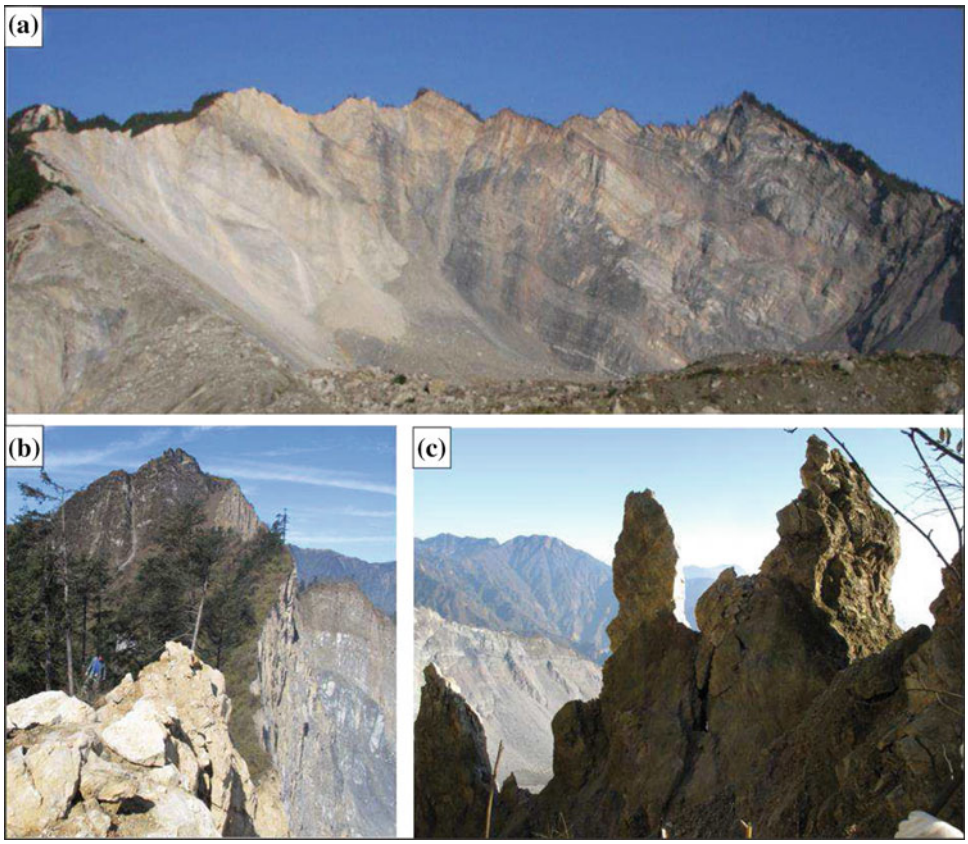

Fig. 2.10 The steep head scarp (**a** and **b**) and the tensile cracks and some fractured rock mass remained in the rear of the landslide (**c**)

(2) *Shattering*

At the same time of the cracking stage, the ground shaking may also cause the shattering of rock mass, accompanied by reducing of the frictional strength and cohesion of the substrate. In the bedrock area with steep dip angle, the slope failure will occur along the bedding weak plane, i.e. the interface between soft and hard rock, intra-formational weak plane.

(3) *Shearing*

For rockslides in dipping strata or slides that may develop tracking the existing structure surface, the shearing failure may occur along the sliding surface driven by the seismic force and self-weight of sliding body. The pre-stage tensile cracking and shattering favors the shearing failure.

The mechanism and dynamics process of the tension cracking-shattering-shearing can be summarized as the "conceptual model" shown in Fig. 2.11. Compared with the common gravity landslides, most of the seismically-induced landslides are characterized by high and steep back scarp with tension cracking formed by horizontal seismic force. In addition, Fig. 2.11 shows that earthquake-triggered landslides are more likely to have larger volume and longer runout distance than the normal gravitational landslides.

Because of the steep slip surface and in addition the dynamics function of the seism, the shattering and loose slope body cannot be retained on sliding surface. So it rushes down so as to form collapse. Because there is no resistance before it, it slides long distance at high speed.

2.3.3 Slope Response to Seismic Waves

The site amplification effect of seismic waves has been commonly accepted as a crucial factor for coseismic landslide occurrence. However, it is still poorly understood, because of the scarcity of accelerometer recordings on slopes. In order to a better understanding of the slope behavior under seismic loading, we monitored a large number of aftershocks after the Wenchuan earthquake and also carried out large-scale shaking table tests.

2.3.3.1 Monitoring of Aftershocks

Five monitoring stations were set up in Dongshan and Shiziliang mountains in Qingchuan County in September 2009, as shown in Figs. 2.12 and 2.13. More than 60 aftershocks have been recorded by 24 January 2010.

Monitoring stations #1, #2 and #3 are equipped in Dongshan mountain at levels of 788 m, 871 m and 962 m above sea level, respectively. Monitoring stations #4 and #5 are located in Shiziliang at 893 m and 962 m, respectively

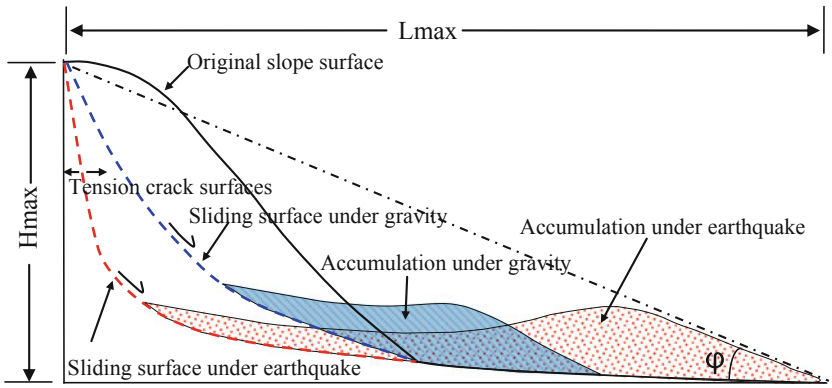

Fig. 2.11 Sketch showing the tension-shattering-shearing failure of earthquake-triggered landslides and the consequent different geomorphic features different from those of landslides under normal gravity conditions

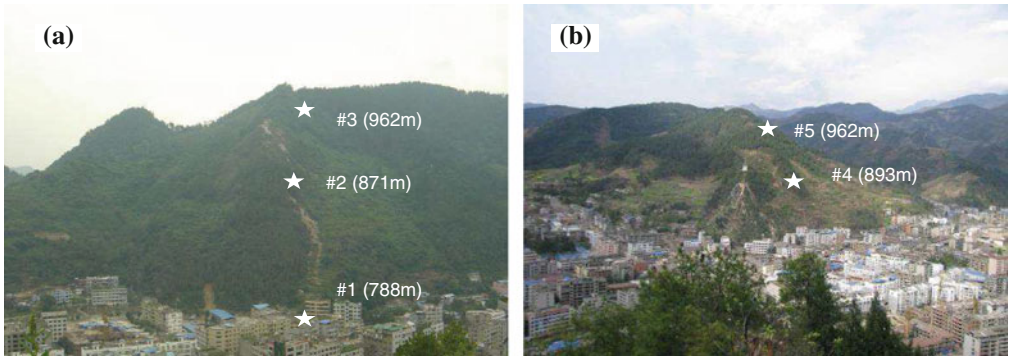

Fig. 2.12 Topography of Dongshan and Shiziliang mountains where monitoring stations are equipped: (**a**) Dongshan; and (**b**) Shiziliang

Fig. 2.13 The monitoring profile

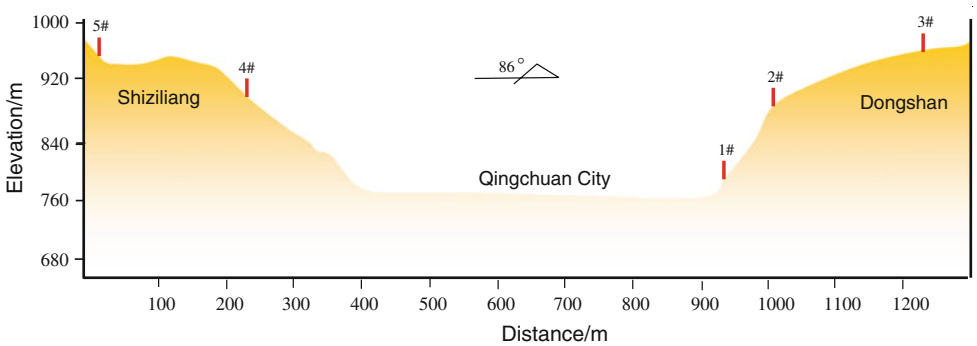

(Fig. 2.12). Qingchuan County is situated to the north of Longmen mountain orogenic belt. Dongshan and Shiziliang mountains are located between the central and southern branches of Qingchuan-Pingwu fault, the mountain trend is nearly in EW direction. During the Wenchuan earthquake both Dongshan and Shiziliang had strong dynamic responses, as a number of collapses or cracks formed there.

Figure 2.14 shows the typical aftershock waves in time domain, monitored by the five stations. Taking the recorded PGA of #1 (788 m) as reference, the ratio of PGA at #2 (871 m) and #3 (962 m) are calculated and shown in Fig. 2.15. The peak horizontal accelerations in east-west direction (a_{EW}) and north-south direction (a_{NS}) are directly from the monitoring. The resultant horizontal acceleration PHA = Max $(\sqrt{aE - W(i)^2} + aN - S(i)^2)$. The overall ground acceleration PGA_0 = Max $(\sqrt{aE - W(i)^2} + aN - S(i)^2 + aU - D(i)^2)$, where $a_{U\text{-}D}$ is the monitored PGA in vertical direction.

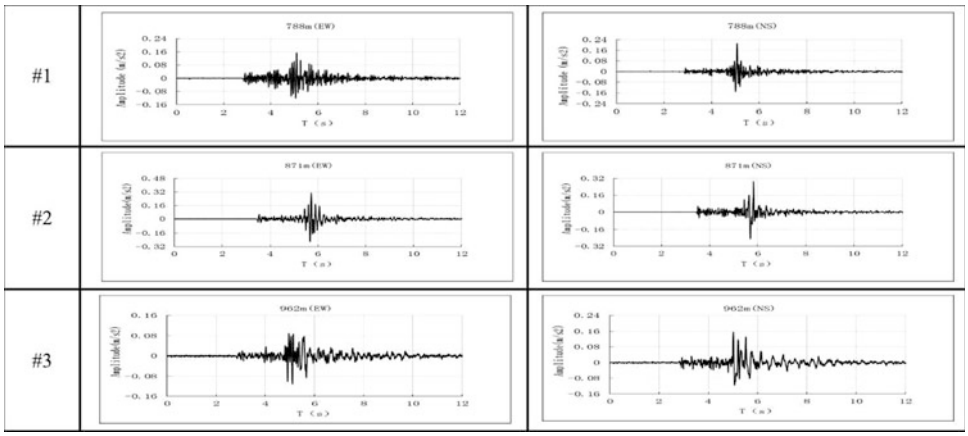

Fig. 2.14 Typical aftershock waves monitored

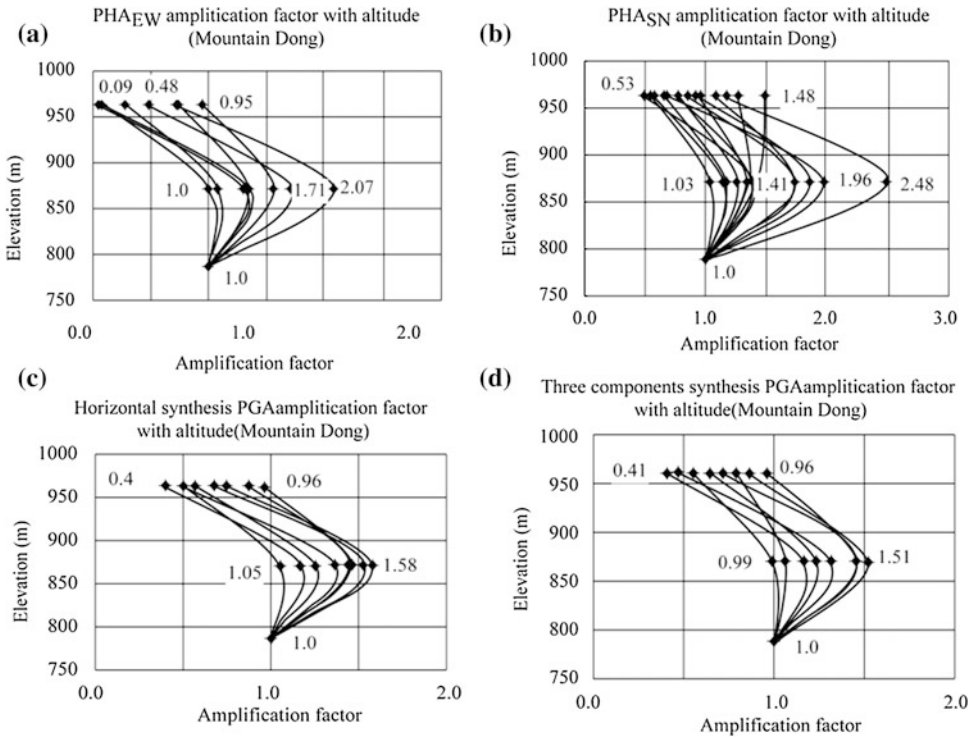

Fig. 2.15 The ratio of PGA at #2 and #3 to that at #1: **a** aEW; **b** aNS; **c** PHA; and **d** PGA

As shown in Fig. 2.15, the ratio of PGA shows a concave pattern with the increase in elevation. The maximum values appear at #2 monitoring station while the minimum values appear at #3, the highest station. As shown in Figs. 2.12 and 2.13, Stations #1 and #2 are at the same slope section, with an almost constant slope angle of about 50°, of Dongshan mountain ridge. Station #3 however, is located at a relatively flat slope section, with a gentle slope angle of about 10 degrees. The relief between #2 and #1 is 83 m and that between #3 and #2 is 91 m. Figure 2.15 infers that (1) peak ground acceleration may be magnified with elevation, as indicated by the relatively high value of PGA at #2 compared with #1; (2) however, sudden change of the slope angle (local topography) may alter the magnification effect of elevation, as PGA at #3 is the minimum though it is the highest station; and (3) the influence of local topography seems to take the higher priority on magnifying PAG than that of elevation.

PGA ratios for monitoring stations #4 and #5 are also derived by taking #1 as reference (Fig. 2.16). Again the PGA ratio shows a concave pattern with elevation. However it decreases first with the minimum values at monitoring station #4. For each aftershock, the lowest station #1 had the biggest PGA; station #4 at the middle level has the lowest PGA; while station #5 at the highest level has the moderate value. The relative low value of PGA at station #5, compared with #1, is thought to be due to the flat stage where station #5 is located (Fig. 2.13).

This is in good agreement with what is observed from monitoring stations in Dongshan mountain (Fig. 2.15). The

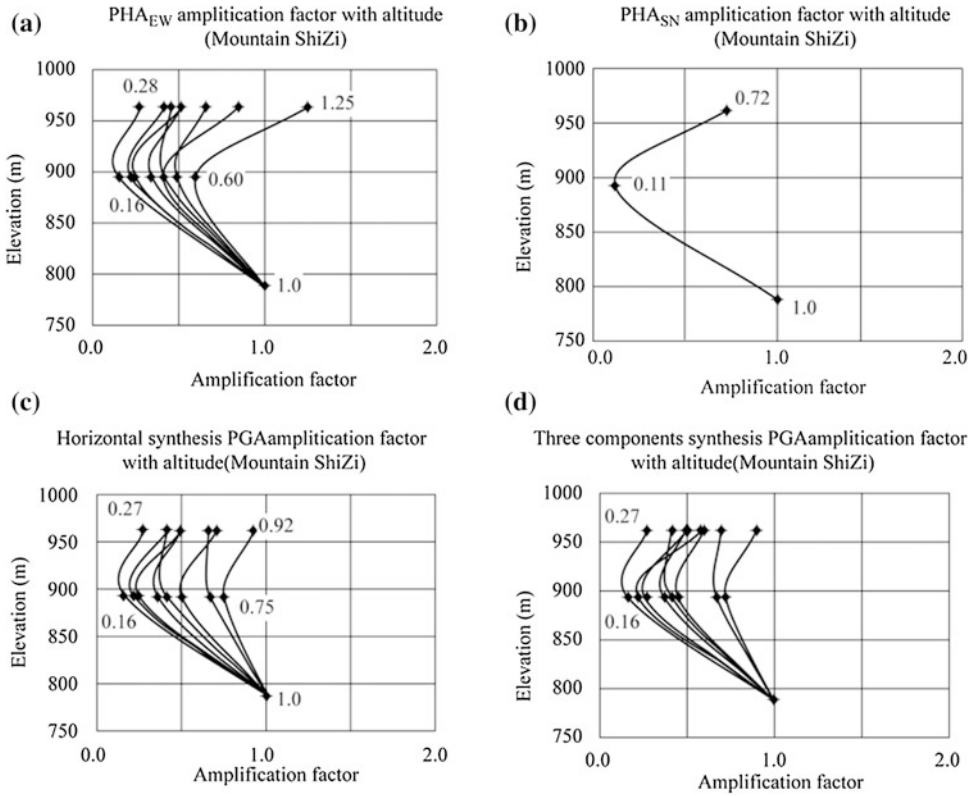

Fig. 2.16 The ratio of PGA at #4 and #5 to that at #1: **a** aEW; **b** aNS; **c** PHA; and **d** PGA

lowest value at station #4 is considered to be attributed to the profile of the slope where the station is located. As shown in Fig. 2.12, station #4 is placed in a concave-shaped slope, which is surrounded by the Shiziliang ridge to the south and a small-scale ridge to the north. Both ridges minimize the degree of freedom of the slope and therefore amplify the response to earthquake vibration. Observations from monitoring of Shiziliang again confirmed that the local topography has priority over elevation in controlling the response of geological body to earthquake vibration.

2.3.3.2 Large-Scale Shaking Table Tests

In order to figure out the dependency, of slope response to earthquake wave, on lithology and slope structure, shaking table tests are conducted. Totally four models are set up for simulating the frequently encountered slopes in the Wenchuan earthquake disaster area, that is consequent bedding slope of hard rock (CH), anti-dip bedding slope of hard rock (ADH), consequent bedding slope of soft rock (CS), and anti-dip bedding slope of soft rock (ADS).

The set-up of shaking table tests is shown in Fig. 2.17. The Buckingham's π theorem is employed as the similarity rule for preparing the models. Dimentional parameters, length L, density ρ and elasticity modulus E, are choosen as the fundamental quantities with scaling factors of CL = 100, Cρ = 1, and CE = 100, respectively. The similarity constants of all key parameters are listed in Table 2.5, and the physical properties of the model material are listed in Table 2.6.

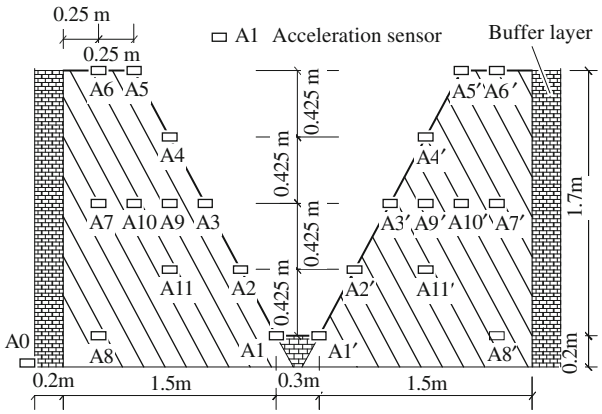

Fig. 2.17 Model layout in shaking table test

Barite powder, quartz sands, gypsum, glycerol and water are mixed in weight proportions of 43.2:30.9:12.3:8.6:1.2 to produce the high strength material of model slopes which simulates hard rock, while a mixture of the same components in proportions of 51.3:32.1:9:6.4:1.3 are to make the low strength materials, which simulates the soft rock. Note that the above proportions are determined through try and error. The barite powder (maximum particle size of 0.074 mm) and quartz sands (0.074–0.85 mm) work as fines and coarse aggregates in the mixture, and the gypsum and water work together as cement. Glycerol was used to slow down the curling of the mixture, in order to achieve the desired strength. Direct shear tests in accordance with

Table 2.5 Similarity constants of the model

Quantities	Similarity ratio	Constants
Geometry size (L)	C_L = 100 (controlled quantity)	100
Density (ρ)	C_ρ (controlled quantity)	1
Acceleration (a)	C_a = 1 (controlled quantity)	1
Weight (γ)	$C_\gamma = C_\rho$	1
Elastic modulus (E)	$C_{E\ =}\ C_\rho C_L$	100
Poisson's ratio (μ)	$C_\mu = 1$	1
Cohesion (C)	$C_C = C_\rho C_L C_a$	100
Friction angle (φ)	$C_\Phi = 1$	1

Table 2.6 Model material parameter table

Lithology	Hard rock		Soft rock	
Type	Prototype	Model	Prototype	Model
Density (KN/m^3)	26.5–27.5	27	26–27	26
Elastic modules (MPa)	6000–9000	73.7	1000–3000	24.1
Poisson's ratio	0.25	0.25	0.28	0.28
Cohesion (MPa)	5–50	0.12	0.5–5	0.043
Friction angle (°)	38–45	43	30–38	35
Joint Cohesion (MPa)	0.5–1.0	0.006	0.05–0.5	0.001
Joint Friction angle (°)	35–40	37	25–30	25

Chinese Standard for Soil Test Method (GB/T 50123-1999) were conducted to obtain the cohesions and internal friction angles of the mixture, and uniaxial compression strength tests in accordance with Standard for Soil Test Method (GB/T 50123-1999) were conducted to obtain the elasticity modulus. The mechanical properties of the interfaces between layers were obtained through direct shear tests (GB/T 50123-1999). The properties of materials for model slopes are listed in Table 2.6.

The hard rock slope is built with prefabricated solid blocks, and the soft rock slope is built in layers. Constructed slopes are put into 2 rigid steel cubes with 20 cm cushioning layer to avoid boundary effect (Fig. 2.18). 42 acceleration monitor devices are installed inside these slopes (Fig. 2.17).

Actual seismic wave from Wolong station during the Wenchuan earthquake are applied to the above built models, and the acceleration are changed gradually from 0.1 to 0.6 g. PGA ratios for each monitoring sensor are calculated by taking the PGA value from sensor A8 as reference. The PGA ratios are plotted in Figs. 2.19 and 2.20.

Generally speaking, the PGA ratios increase with elevation of sensors (both inside the slope and on the slope surface). This indicates an amplification of PGA with elevation, which coincides with the observation from in situ monitoring (Figs. 2.15 and 2.16). The increasing pattern of PGA ratio for sensors inside the slope is consistent in both consequent and anti-dip slopes. However, the increasing patterns for sensors on slope surface are different. In the case of consequent slope, the amplification effect becomes strong at the half height of the slope, where PGA ratios reach as much as 2. In the anti-dip slope, the amplification gets significant at about 2/3 slope height, where PGA ratios reach the value

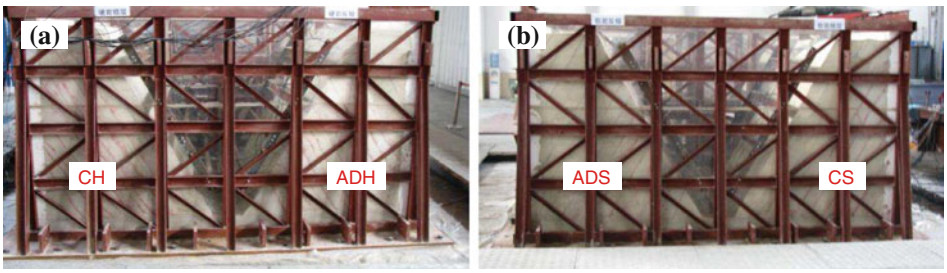

Fig. 2.18 Shaking table test models: **a** hard rock slope; and **b** soft rock slopes

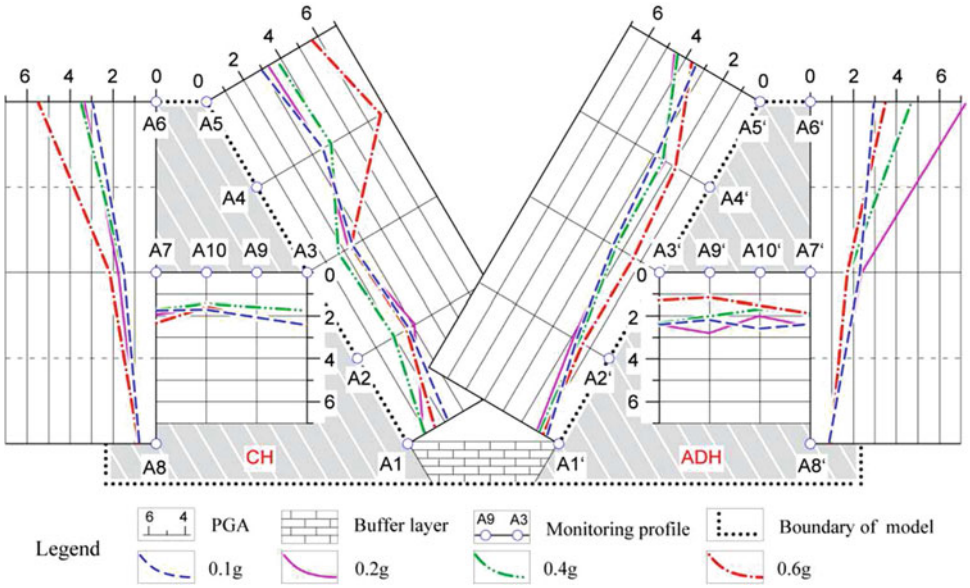

Fig. 2.19 PGA ratios in models of hard rock (*blue line* for acceleration = 0.1 g, *purple* for 0.2 g, *green* for 0.4 g, and *red* for 0.6 g)

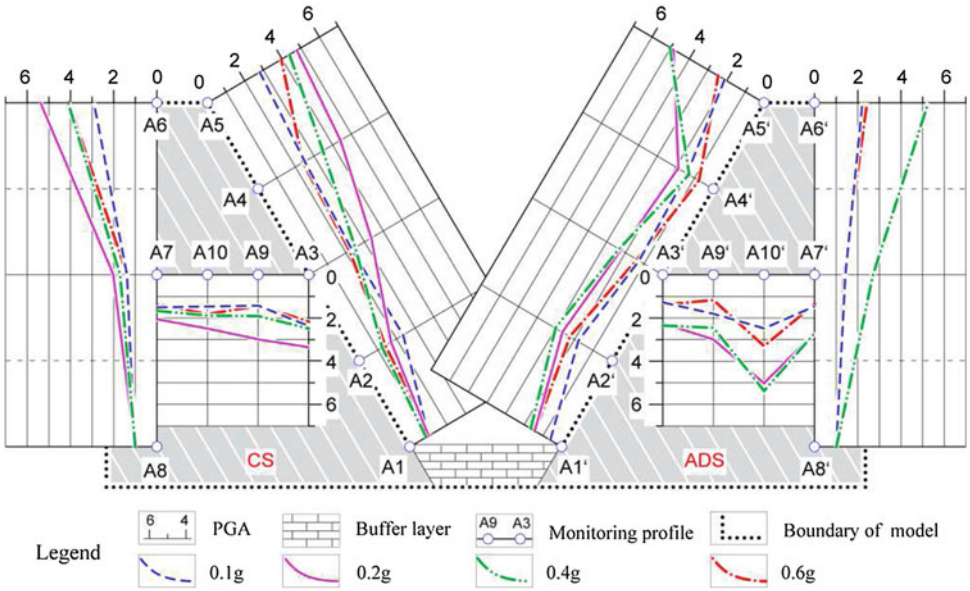

Fig. 2.20 PGA ratios in models of soft rock (*blue line* for acceleration = 0.1 g, *purple* for 0.2 g, *green* for 0.4 g, and *red* for 0.6 g)

of 2. This indicates it is easier for the upper half of consequent slopes to fail in shallow surface during earthquake, while the top one third of anti-dip slope is susceptible to deep failure. On the other hand, the PGA ratio on consequent slope surface is generally greater than that on anti-slip slope surface. This may infer that consequent slope is more sensitive to earthquake vibration than anti-dip slopes.

PGA ratios in models of soft rock are shown in Fig. 2.20. Generally speaking, the PGA ratios (both inside the slope and on the slope surface) increase with elevation. This is in good agreement with what has been observed from the hard rock models as shown in Fig. 2.19. PGA ratios of the surface of consequent slope gradually increase from the bottom to the crest, while sudden increase of PGA ratios happens at the top third part of the anti-dip slope. In addition, the maximum PGA ratios in consequent slope are greater than that in anti-dip slope. This implies that the surficial part of consequent slope is sensitive to earthquake waves, so is the top third part of anti-dip slope.

Based on the foregoing discussion, couple of inferences can be made: (1) the PGA increases with elevation of the subjected slope, regardless of the slope material and structure; and (2) the shallow surface of consequent slope is susceptible to earthquake vibration, so is the top third of anti-dip slope. This may explain the phenomena in field investigation that collapse in shallow surface is concentrated in consequent slope, while deep-seated landslides occur the most in anti-dip slopes.

2.4 Discussions and Conclusion

Based on the research results, the following understanding and conclusions can be drawn for large-scale rock landslides in southwestern China:

(1) The generation of large-scale landslides involves a breakthrough of the sliding plane. The formation and breakthrough of the sliding plane represents a progressive destruction. Based on investigations of recently occurred large-scale landslides, we found two new failure mechanisms: locking-section dominated failure and deep toppling.

(2) The mechanisms of large-scale landslides can be grouped into several typical types: sliding-tension cracking–shearing, retaining wall collapse, soft base collapse, large-scale toppling in interlayered rocks, toppling due to soft base, toppling and dislocation. Each type occurs under certain rock structure conditions and has a specific evolution and failure mechanism.

(3) Large-scale rock landslides always occur with the abrupt brittle failure of a locking section in the slope. The locking section plays an important role in restricting the landslide deformation and improving the stability of a landslide area. It is also the key to evaluating and mitigating landslide disasters.

(4) In anti-inclined lamellar rock slopes, the toppling deformation is closely related to the strength and thickness of the rock. The toppling deformation usually occurs where weak perpendicular planes occur. Investigations also indicate that toppling deformations towards the free face occurred in all steep slate and schist strata, although the toppling degree and scale varied from one slope to another.

(5) Generally, all large-scale and deep-seated toppling deformation failures have a long incubation period. The rock strata may experience large flexible bending deformations and failure only occurs when the deformation accumulates to a certain critical value. In other words, the formation of the sliding plane is part of the evolution of the slope. This must be distinguished from the mechanism of a cataclinal rock slope moving along a potential sliding plane. Most slopes have distortion features, but only a small number evolve into landslides. Once the landslides are formed, they are likely to be large deep slides, due to the long-term geological accumulation.

(6) Toppling failures commonly occur in steep, hard layered strata. Usually, the deformation depth is between 30 and 40 m. Unlike the deformation of soft strata, in hard lamellar rock the deformation involves bending of the joints and cracks. The former has a long deformation time from the beginning to the slope failure, and the degree of toppling can be very large. In contrast, the hard rock strata fail very shortly after the slope begins to deform.

(7) Earthquake-triggered landslides are different from gravitational landslides, normally characterized by serrated, rough, and steep scarps due to the tension cracking caused by the horizontal seismic force. They are also attributed by special failure mechanism and dynamic processes. Based on intensive investigations of a large number of landslides triggered by the Wenchuan earthquake, three basic failure modes are proposed: tensile cracking, shattering and shearing. The failure mechanism of most large-scale landslides can be explained by one mode or the combination of several modes.

(8) The seismic wave propagates to discontinuities in rock slopes, which may cause the tension stress at interfaces and form the tension fractures, because the horizontal seismic force may enormously exceed the tension strength of the rock mass. Meanwhile, the ground shaking may also cause the shattering of rock mass, accompanied by reducing of the frictional strength and cohesion of the substrate. The pre-stage tensile cracking and shattering favors the shearing failure of landslides eventually.

(9) The aftershock monitoring and large-scale shaking table tests have been carried out to better understand the slope response to seismic wave. We found that factors contributing to susceptibility of a certain area to earthquake-induced landslides are ranked as follows: (1) distance from seismic fault deserves the first priority for determining the occurrence and distribution of most of large-scale landslides; (2) profile of the slope gets the second considering its domination of slope's capacity to withstand a shaking, as a concave-shaped slope (generally with low degree of freedom) is found to be less sensitive to earthquake vibrations than a mountain ridge; (3) slope angle may hold the third in its way to alter the pattern of peak ground acceleration, as relatively low PGA generally develops in slope sections dipping less than 10°; and (4) elevation grasps the fourth, as PGA is usually amplified with elevation of a certain slope. In addition, consequent slope and anti-dip slope are found to exhibit different behavior during earthquake shaking. The shallow surface of consequent slope is susceptible to earthquake shaking, so is the top third of anti-dip slope. This coincides with the phenomena in field investigation that collapse in shallow surface is concentrated in consequent slope, while deep-seated landslides occur the most in the anti-dipping slopes.

Acknowledgment This study is financially supported by the National Basic Research Program of China (973 Program) (Grant No.2013CB733202) and the Key Project of National Natural Science Foundation of China (Grant No.41130745). The author would like to acknowledge the assistance of Dr. Xuanmei Fan, Dr. Rongyan Li, Dr. Yonghong Luo and Dr. Guo Li of Chengdu University of Technology, who provided help for the paper organization and English editing.

2.5 Appendix A: 50 historical catastrophic landslides in recent 100 years

No.	Time	Name	Location	Longitude	Latitude	Fatalities	Triggering factor
1	1905/6/9	Nanmenwan landslide	Wuxi, Chongqing	109.6301	31.3955	98	Rainfall
2	1921/7/18	Pufugou landslide	Luquan, Yunnan	102.5962	26.1686	7	Rainfall
3	1935/11/25	Luchedu landslide	Huidong, Sichuan	102.3144	26.1927	286	Rainfall
4	1935/12/22	Shabagou landslide	Qiaojia, Yunnan	102.9950	27.0077	280	Rainfall
5	1942/7/1	Jiawucun landslide	Xide, Sichuan	102.3175	28.0542	190	Rainfall
6	1943/1/3	Chana landslide	Gonghe, Qinghai	100.8067	36.0678	114	Snowmelt
7	1956/8/3	Langjiaogou landslide	Pingshun, Shanxi	113.5707	36.3433	92	Rainfall
8	1961/3/6	Tangyanguan landslide	Anhua, Hunan	111.1108	28.3137	40	Impoundment
9	1963/7/9	Wudangqu landslide	Guiyang, Guizhou	106.7708	26.6188	7	Rainfall
10	1964/7/20	Hongshuigou landslide	Lanzhou, Gansu	103.5881	36.0637	157	Rainfall
11	1965/11/20	Lannigou landslide	Luquan, Yunnan	102.5964	26.1716	444	Rainfall
12	1996/12/4	Shachonglu landslide	Guiyang, Guizhou	106.6912	26.5461	35	Slope cutting
13	1970/5/26	Lugutiekuang landslide	Mianning, Sichuan	102.2577	28.2852	104	Rainfall
14	1971/8/16	Maidi landslide	Hanyuan, Sichuan	102.7052	29.3727	40	Irrigation
15	1974/9/14	Baimeiya landslide	Nanjiang, Sichuan	106.9991	32.4462	159	Rainfall
16	1980/6/3	Yanchihe rockfall	Yuan'an, Hubei	111.2998	31.2086	281	Underground mining
17	1982/7/18	Jipazi landslide	Yunyang, Chongqing	108.7430	30.9282	0	Rainfall
18	1983/3/7	Saleshan landslide	Dongxiang, Gansu	103.5837	35.5707	240	Rainfall
19	1983/7/2	Laojia landslide	Qiaojia, Yunnan	102.9780	26.9438	32	Rainfall
20	1983/7/29	Zhongtingxiang landslide	Wanyuan, Sichuan	108.4235	32.1067	7	Rainfall
21	1983/8/31	Fengshanfenkuang landslide	Yimen, Yunnan	101.9507	24.6605	11	Underground mining
22	1985/8/21	Dapingshan landslide	Tengchong, Yunnan	98.4241	25.5115	22	Rainfall
23	1988/1/10	Zhongyangcun-1 landslide	Wuxi, Chongqing	109.5229	31.5836	33	Blasting
24	1989/7/10	Xikou landslide	Huaying, Sichuan	106.7261	30.1740	221	Rainfall
25	1991/6/17	Donglongshan landslide	Wushan, Chongqing	109.9908	31.0631	7	Underground mining
26	1991/9/23	Touzhaigou landslide	Zhaotong, Yunnan	103.8542	27.5676	216	Rainfall
27	1994/4/30	Jiguanling rockfall	Wulong, Chongqing	107.494	29.4685	16	Underground mining
28	1996/6/3	Laojinshan landslide	Yuanyang, Yunnan	103.1305	22.8554	227	Underground mining
29	1996/9/19	Yankou landslide	Yinjiang, Guizhou	108.4423	27.9936	3	Rainfall
30	1997/6/5	Bo'amo landslide	Meigu, Sichuan	103.2875	28.1215	150	Rainfall
31	1998/5/22	Yanxihe landslide	Nanjiang, Sichuan	106.5988	31.9935	0	Rainfall
32	1998/5/1	Gangkouzhen landslide	Wulong, Chongqing	107.7453	29.3312	79	Rainfall
33	2000/4/9	Yigong landslide	Bomi, Tibet	94.9914	30.2422	0	Snowmelt
34	2000/6/6	Shuangliu landslide	Gulin, Sichuan	106.1757	27.9298	10	Rainfall
35	2000/8/14	Yingjiang landslide	Yingjiang, Yunnan	97.9822	24.7591	13	Rainfall
36	2003/7/13	Qianjiangping landslide	Zigui, Hubei	110.6023	30.9757	24	Rainfall
37	2004/9/5	Tiantaixiang landslide	Xuanhan, Sichuan	108.0571	31.4355	0	Rainfall
38	2004/12/3	Yanjiao rockfall	Nayong, Guizhou	105.2484	26.6974	44	Rainfall
39	2007/7/7	Bao'eryan landslide	Daxian, Sichuan	107.4635	31.5103	0	Rainfall
40	2007/7/19	Sujiahedianzhan landslide	Tengchong, Yunnan	98.2578	25.3392	29	Slope cutting
41	2007/11/20	Gaoyangzhai landslide	Badong, Hubei	110.3288	30.6227	35	Rainfall

(continued)

(continued)

No.	Time	Name	Location	Longitude	Latitude	Fatalities	Triggering factor
42	2009/4/26	Yangtiyan landslide	Zhaotong, Yunnan	105.0540	27.8591	20	Rainfall
43	2009/6/5	Jiweishan landslide	Wulong, Chongqing	107.4329	29.2322	74	Underground mining
44	2009/8/6	Houziyan landslide	Hanyuan, Sichuan	102.7819	29.3131	31	Rainfall
45	2010/6/14	Shuangjigou landslide	Kangding, Sichuan	102.2894	30.4354	23	Rainfall
46	2010/6/28	Guanling landslide	Guanling, Guizhou	105.3302	25.9564	99	Rainfall
47	2010/7/27	Ermanshan landslide	Hanyuan, Sichuan	102.7439	29.3225	20	Rainfall
48	2010/9/1	Dashifang landslide	Baoshan, Yunnan	98.9863	25.5744	48	Rainfall
49	2011/9/17	Bailuyuan landslide	Xi'an, Shaanxi	109.1	34.2667	32	Rainfall
50	2013/7/10	Wulipo landslide	Sichuan	103.57	30.91	148	Rainfall

References

Chen XL, Zhou Q, Ran H, Dong R (2012) Earthquake-triggered landslides in southwest of China. Nat Hazards Earth Syst Sci 12:351–363

Dai FC, Xu C, Yao X, Xu L, Tu XB, Gong QM (2011) Spatial distribution of landslides triggered by the 2008 Ms 8.0 Wenchuan earthquake, China. J Asian Earth Sci 40(4):883–895

Duan YH (2000) Present state, trend and countermeasure of geological hazards in Chinese West. Econ res ref 58(2):12–18

Earthquake disaster prevention department of China Earthquake Administration (1999) Catalogue of modern earthquakes in China. China Science and Technology Press, Beijing (in Chinese)

Fan X, van Westen CJ, Xu Q, Görüm T, Dai F (2012a) Analysis of landslide dams induced by the 2008 Wenchuan earthquake. J Asian Earth Sci 57:25–37

Fan X, Tang CX, van Westen CJ, Alkema D (2012b) Simulating dam-breach scenarios of the Tangjiashan landslide dam induced by the Wenchuan earthquake: Natural Hazards and Earth System Sciences 12:3031–3044

Fan X, van Westen CJ, Korup O, Görüm T, Xu Q, Dai F, Huang R, Wang G (2012c) Transient water and sediment storage of the decaying landslide dams induced by the 2008 Wenchuan earthquake, China. Geomorphology 171–172:58–68

Fan X (2013) Understanding the causes and effects of earthquake-induced landslide dams. Ph.D thesis, University of Twente, p 209. ISBN: 978-90-6164-361-6

Görüm T, Fan X, van Westen CJ, Huang RQ, Xu Q, Tang C, Wang G (2011) Distribution pattern of earthquake-induced landslides triggered by the 12 May 2008 Wenchuan earthquake. Geomorphology 133(3–4):152–167

Huang RQ, Deng RG et al (1993) Full simulation process for high slope substance moving. Chengdu University of Technology Press, Chengdu

Huang RQ (1996a) Studies of the geological model and formation mechanism of Xikou landslide. In: Balkema AA (ed) Proceedings of the 7th international symposium on landslides, pp 1671–1678

Huang RQ (1996b) Full-course numerical simulation of hazardous landslides and falls. In: Balkema AA (ed) Proceedings of the 7th international symposium on landslides, pp 1134–1140

Huang RQ, Wang ST, Zhang ZY et al (2002a) Shallow earth crust dynamics process and engineering environment research in Western China. Sichuan University Press, Chengdu

Huang RQ, Chen LS (2004) Human induced landslide in China: mechanism study and its implications on slope management. Chin J Rock Mech Eng 23(16):2766–2777

Huang RQ (2009) Some catastrophic landslides since the twentieth century in the southwest of China. Landslides 6:69–81

Huang RQ, Li WL (2009a) Analysis of the geo-hazards triggered by the 12 May 2008 Wenchuan Earthquake, China. Bull Eng Geol Environ 68(3):363–371

Huang RQ, Li WL (2009b). A study on the development and distribution rules of geo- hazards triggered by "5.12"Wenchuan earthquake. Sci China (edition E) 52(4):810–819

Huang RQ (2011) Geo-engineering lessons learned from the 2008 Wenchuan earthquake in Sichuan and their significance to reconstruction. J Mt Sci 8:176–189

Huang RQ (2012) Mechanism of large-scale landslides in China. Bull Eng Geol Environ 71:161–170

Huang RQ, Pei X, Fan X, Zhang W, Li S, Li B (2012) The characteristics and failure mechanism of the largest landslide triggered by the Wenchuan earthquake (May 12, 2008). China. Landslides 9(1):131–142

Huang R, Fan X (2013) The landslide story. Nat Geosci 6(5):325–326

Huang RQ, Zhao JJ, Ju NP, Li G, Lee LM, Li YR (2013) Analysis of an anti-dip landslide triggered by the 2008 Wenchuan earthquake in China. Nat Hazards 68:1021–1039

Huang ZZ, Tang RC, Liu SL (2002b) Re-discussion of the seismogenic structure of the Diexi large earthquake in 1933 and the Arc tectonics on Jiaochang, Sichuan Province. Earthq Res China 18(2):183–192

Jiang CS (2000) Present state and prevention of China's geological disasters. Chin Geol 48(4):3–5

Keefer DK (1984) Landslides caused by earthquakes. Geol Soc Am Bull 95(4):406–421

Li N (1992) Landfall-landslide blocking river disasters and its prevention measures in Yunnan Province[C]. Commission of Proceedings of Landslides edn. Proceedings of Landslides (No. 9), China Railway Publishing House, Beijing, pp 50–55

Lin A, Ren Z, Jia D, Wu X (2009) Co-seismic thrusting rupture and slip distribution produced by the 2008 M_w 7.9 Wenchuan earthquake, China. Tectonophysics 471(3–4):203–215

Liu C, Li W, Wu H., Lu P, Sang K, Sun W, Chen W, Hong Y, Li R (2013). Susceptibility evaluation and mapping of China's landslides based on multi-source data. Nat Hazards. DOI 10.1007/s11069-013-0759-y

Schuster RL (1996) The 25 most catastrophic landslides of the 20th century. In: Chacon J, Irigaray C, Fernandez T (eds) Landslides, Proceedings of the 8th international conference and field trip on landslides, Granada, Spain, Balkema, Rotterdam, 27–28 Sept 1996

Shen ZK, Sun J, Zhang P, Wan Y, Wang M, Burgmann R, Zeng Y, Gan W, Liao H, Wang Q (2009). Slip maxima at fault junctions and rupturing of barriers during the 2008 Wenchuan earthquake. Nature Geosci 2(10):718–724

Tang C, Zhu J, Qi X, Ding J (2011) Landslides induced by the Wenchuan earthquake and the subsequent strong rainfall event: a case study in the Beichuan area of China. Eng Geol 122(1–2):22–33

Tang C, Van Asch ThWJ, Chang M, Chen GQ, Zhao XH, Huang XC (2012) Catastrophic debris flows on 13 August 2010 in the Qingping area, southwestern China: the combined effects of a strong earthquake and subsequent rainstorms. Geomorphology 139–140:559–576

The U.S. Geological Survey (2000) Landslide hazards. USGS Fact Sheet Fs-071-00

Wang SJ (1992) The deformation mechanism and process research of Jinchuan strip mine slope. Chin J Geotech Eng 14(1):1–7

Wang SJ (1999) Tasks and future of engineering geology. J Eng Geol 7 (3):195–199

Wang ST, Huang RQ, Li YS (1995) Key engineering geology problems and research on Jinping Hydropower Station in Yalongjiang River. Chengdu University of Science and Technology Press, Chengdu (in Chinese)

Xu Q, Chen JJ, Feng WK, Xiao RH, Zuo YY (2009a) Study of the seismic response of slopes by physical genetic types of large-scale landslides modeling. J Sichuan Univ (Eng Sci Ed) 41(3):266–272 (in Chinese with English abstract)

Xu Q, Pei XJ, Huang RQ (2009b) Large-scale landslides induced by the Wenchuan Earthquake. Science Press, Beijing (in Chinese)

Xu Q, Fan X, Huang RQ (2009c) Landslide dams triggered by the Wenchuan Earthquake, Sichuan Province, south west China. Bull. of Engineering Geology and the. Environment 68(2):373–386

Xu Q, Shang Y, van Asch T, Wang S, Zhang Z, Dong X (2012) Observations from the large, rapid Yigong rock slide—debris avalanche, southeast Tibet. Can Geotech J 49(5):589–606

Xu Q, Zhang S, Dong XJ (2013) Genetic types of large-scale landslides induced by the Wenchuan earthquake. In: Ugai K, Yagi H, Wakai A (eds) Earthquake-induced landslides, proceedings of the international symposium on earthquake-induced landslides, Kiryu, Japan, 2012, pp 511–520

Xu X, Wen X, Yu G, Chen G, Klinger Y, Hubbard J, Shaw J (2009d) Coseismic reverse- and oblique-slip surface faulting generated by the 2008 M_w 7.9 Wenchuan earthquake, China. Geology 37 (6):515–518

Yin YP (2001) A review and vision of geological hazards in China. Manage Geol Sci Technol 18(3):26–29

Yin YP, Wang F, Sun P (2009) Landslide hazards triggered by the 2008 Wenchuan earthquake, Sichuan, China. Landslides 6 (2):139–152

Yin YP (2010) Mechanism of apparent dip slide of inclined bedding rockslide-a case study of Jiweishan rockslide in Wulong, Chongqing. Chin J Rock Mech Eng 29(2):18–29

Yu B, Ma Y, Wu YF (2010) Investigation of severe debris flow hazards in Wenjia gully of Sichuan Province after the Wenchuan Earthquake. J Eng Geol 18(6):827–836 (in Chinese with English abstract)

Zhang ZY, Liu HC (1990) Key engineering geology problem and research on Longyangxia Hydropower Station of Huanghe River. Chengdu University of Technology Press, Chengdu

Zhang ZY, Wang ST, Wang LS (1994) Principle of engineering geology analysis. Geological Publishing House Press, Beijing

Zhou W, Tang C, van Ash TWJ, Zhou C (2014) Rainfall-triggering response patterns of post-seismic debris flows in the Wenchuan earthquake area. Nat Nazards 70:1417–1435

http://www.springer.com/978-3-319-09056-6

Engineering Geology for Society and Territory - Volume 2
Landslide Processes
Lollino, G.; Giordan, D.; Crosta, G.B.; Corominas, J.; Azzam, R.; Wasowski, J.; Sciarra, N. (Eds.)
2015, XLVII, 2177 p. 1567 illus., 1279 illus. in color. In 3 volumes, not available separately., Hardcover
ISBN: 978-3-319-09056-6